Chemical Engineering Research and Design 143 (2019) 215–225

Contents lists available at ScienceDirect

Chemical Engineering Research and Design

journal homepage: www.elsevier.com/locate/cherd

Generalizing the effects of the baffling structures on the buoyancy-induced turbulence in secondary settling tanks with eleven different geometries using CFD models

Haiwen Gao, M.K. Stenstrom *

Dept. of Civil and Environmental Engineering, University of California Los Angeles, 5714 Boelter Hall, Los Angeles, CA 90095, USA

ARTICLE INFO

Article history:
Received 24 September 2018
Received in revised form 12 November 2018
Accepted 14 January 2019
Available online 22 January 2019

Keywords:
Secondary settling tank
Computational fluid dynamics modeling
Effect of buoyancy on turbulence
Internal baffling structures

ABSTRACT

Computational fluid dynamics (CFD) models are applied to understand the effects of baffling structures on the buoyancy-induced turbulence flow in secondary settling tanks (SSTs). Eleven SST geometries, including four circular SSTs and seven rectangular SSTs, are evaluated in this study. The main research tool is a Fluent-based two-dimensional SST model. The model is verified with observations from literature. The validated model is then applied to compare the predictions of the effluent suspended solids (ESS) by the buoyancy-decoupled and buoyancy-coupled turbulence models on each SST geometry. Next, the effects of the SST baffling structures on the turbulence properties are compared and quantified. Additionally, stress tests are simulated on the SSTs, to predict their performances using both the buoyancy-decoupled and buoyancy-coupled turbulence models.

The results for the original flow conditions show that the effects of the SST baffling structures on the buoyancy-induced turbulence can be divided into three zones: Zones A, where the baffling structures have negligible damping effects, and only the buoyancy-coupled turbulence model provides accurate predictions; Zone B, where the baffling structures partially dissipate the effect of buoyancy on turbulence, and the buoyancy-coupled model continues to provide accurate predictions but the buoyancy-decoupled turbulence model only provides qualitative but similar predictions; and Zone C, where the baffling structures fully dissipate the effect of buoyancy on turbulence, and both models provide similar, accurate predictions. Two indicators, the densimetric Froude number and the differences in turbulent kinetic energy can be used to predict the need for buoyancy coupling.

1. Introduction

In conventional wastewater treatment plants (WWTPs), the activated sludge process (ASP) is the most popular technique to remove organic matter and reduce nutrients such as nitrogen and phosphorus (Li and Stenstrom, 2014). After the bio-reaction in the aeration tank, the effluent has a highly concentrated biomass and must be separated by secondary settling tank (SST), also known as secondary clarifier or secondary sedimentation tank.

In order to study the flow field and solids distribution in an SST, computational fluid dynamics (CFD) simulations have been developed in the last 30 years and have become a practical approach. Larsen (1977) was the pioneer in applying CFD to predict the hydrodynamics in settling tanks and set the framework for future CFD settling tank research. Since then, applications of CFD in settling tanks have become popular and have been used to (1) understand the hydrodynamics in the SST (Zhou and McCorquodale, 1992a, 1992b, 1992c; Tamayol et al., 2009); (2) optimize internal structures (Gong et al., 2011; Patziger et al., 2012; Ramalingam et al., 2012; Xanthos et al., 2013; Das et al., 2016; Patziger,

* Corresponding author.
E-mail address: stenstro@seas.ucla.edu (M.K. Stenstrom).
https://doi.org/10.1016/j.cherd.2019.01.015
0263-8762/

2016; Gao and Stenstrom, 2017) and (3) adjust operation process (Parker et al., 2008; Patziger et al., 2008, 2012).

Compared with the experimental study, the main advantages of CFD simulations are less expense and less time commitment. However, because of the limited computational speed and storage in many of the early studies, simple turbulence models, such as constant eddy viscosity model and mixing length theory model were used to qualitatively study the turbulence flow in the SST (Imam et al., 1983; Krebs, 1991; Krebs et al., 1992, 1995). However, the constant eddy viscosity model needs a constant value to estimate the turbulence effects on the flow. The mixing-length model requires an accurate estimate of the mixing length. Neither parameter can be measured directly which means that both models require additional information to estimate these two parameters (McCorquodale et al., 2004). Since the disadvantages of these two models, more advanced turbulence models such as standard k-ε (SKE) model, RNG k-ε model and Realizable k-ε model, have been applied in recent settling tank studies (Zhou and McCorquodale, 1992a; 1992b; 1992c; Vitasovic et al., 1997; Lakehal et al., 1999; Weiss et al., 2007; Patziger and Kiss, 2015; Das et al., 2016).

Gao and Stenstrom (2018a) compared the influences of SKE, RNG k-ε and Realizable k-ε models on the performance of a circular SST using data from Burt (2010), and McCorquodale et al. (2004). Their results showed that turbulence model selection has a strong influence on the prediction of SST capacity and the SST hydrodynamics, especially inside the inlet zone and near the sludge hopper.

Additionally, the applications of turbulence models lack consensus of the use of the buoyancy term (G_b) in the turbulent kinetic energy (TKE). In some early applications of the SKE model, this term was decoupled in the TKE equation. Devantier and Larock (1986) explained that coupling G_b in the TKE equation required solving numerically stiff equations and difficulty in obtaining solution convergence. Some other researches also ignored G_b in the TKE equation (Zhou and McCorquodale, 1992a, 1992b; Vitasovic et al., 1997; Tamayol et al., 2009). Comments on these researches were briefly summarized in Gao and Stenstrom (2018b).

On the contrary, G_b was also widely applied in many other SST studies (Lyn et al., 1992; Dahl, 1993; Lakehal et al., 1999; Xanthos et al., 2010; Shahrokhi et al., 2013; Ramin et al., 2014). Gao and Stenstrom (2018b) studied the effects of the buoyancy-induced turbulence on Darvill SST under varied MLSS concentrations and sludge settling velocities. Only a vertical inlet baffle was installed in the Darvill SST to dissipate the inflow energy. The results showed that installing the inlet dissipating baffle alone cannot reduce the effect of buoyancy on turbulence. For this case and cases like it, the effect of buoyancy on turbulence are negligible only when the loading conditions are limited, often outside of normal operating range.

Since flow in the SST is the turbulent, density-driven flow, understanding the effect of buoyancy on turbulence in different SST geometries is very important. Additionally, decoupling buoyancy in the turbulence model makes the numerical model converge faster than the buoyancy coupled turbulence model; therefore, saving computing time. A predictive tool to show when a decoupled approach will work is of value in saving computing resources and effort.

In this study, 11 different types of the SST geometries, including 4 circular SSTs types and 7 rectangular SSTs types are evaluated to generalize the effects of the internal baffling structures on the buoyancy-induced turbulence in SSTs with different geometries. The following two questions are answered: (1) What parameter can be used to quantify the effects of the baffling structure and to indicate if the G_b-decoupled turbulence model will work under a normal flow conditions? (2) If the G_b-decoupled turbulence model tends to work as the G_b-coupled turbulence model under a normal flow condition in different SST geometries, which parameter can be used to differentiate the performance of the G_b-decoupled/coupled turbulence models, and is useful to compare in different SST geometries?

Firstly, the measurements of the velocity profiles and performance indicators, such as effluent suspended solids (ESS), sludge blanket height (SBH) in the original and the modified Witney SST geometries are used to verify the model predictions. Both the G_b-decoupled/coupled SKE models are verified. Next, the predictions of the ESS by the G_b-decoupled/coupled SKE models for all eleven geometries are compared. Then, the effects of the varied baffling structures on the turbulence properties by the G_b-decoupled/coupled SKE models are analyzed and quantified. Additionally, stress tests are simulated on the Zones B and C by both models.

2. Methodology

2.1. *The mathematical model*

The commercial CFD code ANSYS Fluent (v.17.2) is used to determine the steady-state, turbulent, and density stratified flow in the different SSTs. Consistent with the previous research (Gao and Stenstrom, 2018a, 2018b), the circular SSTs in this research are also investigated by the two-dimensional axisymmetric approach. The major difference is the G_b-decoupled turbulence model is also applied with the G_b-coupled turbulence model. Since the current study focus on the effect of buoyancy on turbulence, only the applied turbulence model is shown below. A more detailed description of CFD model non-Newtonian flow behavior of the activated sludge and sludge settling properties are shown in Gao and Stenstrom (2018a).

The standard k-ε (SKE) model is applied in this study. The transport equations for the turbulent kinetic energy (k) and the turbulent dissipation rate (ε) are shown below:

$$u\frac{\partial k}{\partial r} + v\frac{\partial k}{\partial y} = \frac{\partial}{\partial r}\left[\left(\vartheta + \frac{\vartheta_t}{\sigma_k}\right)\frac{\partial k}{\partial r}\right] + \frac{\partial}{\partial y}\left[\left(\vartheta + \frac{\vartheta_t}{\sigma_k}\right)\frac{\partial k}{\partial y}\right] + G_k + G_b - \rho\varepsilon \quad (1)$$

and:

$$u\frac{\partial \varepsilon}{\partial r} + v\frac{\partial \varepsilon}{\partial y} = \frac{\partial}{\partial r}\left[\left(\vartheta + \frac{\vartheta_t}{\sigma_\varepsilon}\right)\frac{\partial \varepsilon}{\partial r}\right] + \frac{\partial}{\partial y}\left[\left(\vartheta + \frac{\vartheta_t}{\sigma_\varepsilon}\right)\frac{\partial \varepsilon}{\partial y}\right] + C_1\frac{\varepsilon}{k}G_k - C_2\rho\frac{\varepsilon^2}{k} \quad (2)$$

G_k represents the generation of turbulent kinetic energy (TKE) due to the mean velocity gradients, and G_b corresponds to the buoyancy-induced TKE. The SKE model without or with the implementation of the G_b term is named buoyancy-decoupled (G_b-decoupled) or buoyancy-coupled (G_b-coupled) SKE model, respectively.

$$G_k = \vartheta_t\left[2\left(\frac{\partial u}{\partial r}\right)^2 + 2\left(\frac{\partial v}{\partial y}\right)^2 + 2\left(\frac{u}{r}\right)^2 + \left(\frac{\partial u}{\partial y} + \frac{\partial v}{\partial r}\right)^2\right] \quad (3)$$

$$G_b = -g\frac{\vartheta_t}{\sigma_t}\frac{\partial \rho}{\partial y} \quad (4)$$

The turbulent viscosity, ϑ_t, is then determined as a function of k and ε by

$$\vartheta_t = C_\mu\frac{k^2}{\varepsilon} \quad (5)$$

The dimensionless empirical constants are given the standard values suggested by Rodi (1993). $C_\mu = 0.09$, $C_1 = 1.44$, $C_2 = 1.92$, $\sigma_k = 1.0$, and $\sigma_\varepsilon = 1.3$.

Additionally, inlet densimetric Froude number (Fr) is applied in this study to describe the inertial and density gravity force in the SSTs in terms of initial momentum and buoyancy flux. It was applied in the previous studies to describe the

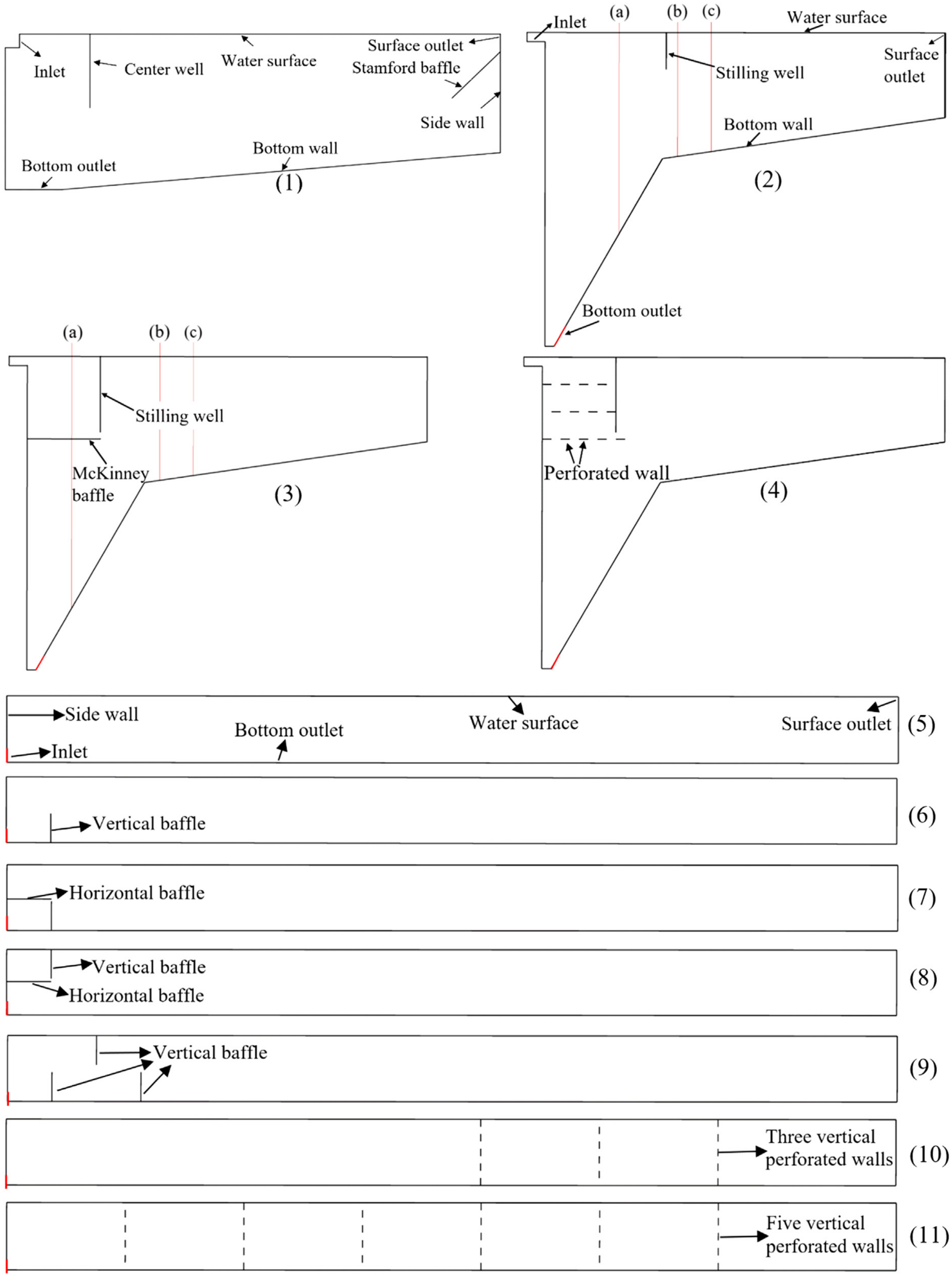

Fig. 1 – Different SST geometries. (a)–(c) in second and third geometries refer to the radial locations for the model verification shown in Fig. 3. Since the geometries No. (3) and (4) are similar to No. (2), only the differences are named in the geometries No. (3) and (4). Similarly, because the geometries No. (6–11) are similar to No. (5), only the differences are named in the geometries No. (6–11).

effects of the bottom density current in SSTs (Zhou et al., 1992) and to optimize the inlet-structure design (Krebs et al., 1995). Since Fr is dimensionless, it can be used to compare the SST performance in difference geometries or loading conditions in this study.

$$F_r = \left(\frac{u_o^2}{gH_{in}\frac{\rho-\rho_r}{\rho_r}} \right)^{½} \quad (6)$$

Where u_o is the inlet velocity; ρ_r is the clear water density; and ρ is the local density of mixture.

Table 1 – Loading conditions of the different cases and their relevant geometries numbers.

Different cases	Relevant geometries shown in Fig. 1	Inflow parameters			Settling parameters[a]			Dry solids density
No.	No.	MLSS g/L	RAS ratio	SOR m/h	V_o m/h	r_h L/g	r_p L/g	ρ_p kg/m^3
Circular SSTs	Circular SSTs							
1	1	4.600	0.80	0.866	7.710	0.390	10.00	
2	2	4.187	1.09	0.332	12.64	0.340	12.25	
3a	3	3.384	1.09	0.332	13.32	0.386	13.00	
3b	3	2.904	0.83	0.673	13.32	0.386	13.00	
3c	3	4.187	1.09	0.332	13.32	0.386	13.00	
4	4	4.187	1.09	0.332	13.32	0.386	13.00	
Rectangular SSTs	Rectangular SSTs							1450
5	5							
6	6							
7	7							
8	8	4.187	0.91	1.01	12.64	0.340	12.25	
9	9							
10	10							
11	11							

[a] V_o is Stokes velocity. r_h and r_p account for rapidly and poorly settling floc, respectively.

2.2. *Geometries and meshing*

Fig. 1 shows 11 different SST geometries. The circular SSTs, geometry No. 1 is the Darvill SST described in McCorquodale et al. (2004), and one loading condition is run for this geometry (Case 1). No. 2 is the old Witney SST, and one loading condition is run with this geometry (Case 2). No. 3 is the new Witney SST, and three loading conditions are run for this geometry (Case 3a–c). Both the old and modified Witney SSTs are described by Burt (2010). No. 4 is a new Witney SST created in this study and one loading condition is run for this geometry (Case 4). Therefore, 6 cases are run with these 4 circular SSTs.

For the rectangular SSTs, geometry No. 5 is the Krebs SST (Krebs et al., 1996). No. 6–11 are the modified Krebs SSTs created in this study. One loading condition is run with each rectangular SST. Therefore, 7 cases are run with these 7 rectangular SSTs (Cases 5–11). Totally, 13 cases are run with these 11 SSTs. Each geometry run one case, except for the geometry No. 3, which run three cases (Case 3a–c). The loading conditions of these 13 different cases and their relevant geometries numbers are listed in Table 1. The dimensions of the four circular and seven rectangular SSTs are shown in Tables 2 and 3, respectively.

In this study, the computational grids for the Darvill SST are approximately 218,700 cells; the Witney SSTs required approximately 428,000 cells and rectangular SSTs require 230,000 cells. These sizes are selected after grid independent tests. The results of grid independent tests on geometries No. 1 and 2 are described in our previous study (Gao and Stenstrom, 2018a). Since the G_b-decoupled turbulence model provide similar, accurate predictions with the G_b-coupled turbulence model on both geometries No. 3 and 4, in order to ensure that the buoyancy effects are reasonably resolved, one coarser mesh (225,000 cells) and one finer mesh (900,000 cells) are used. The differences in the concentration field along the radial direction of circular SSTs on geometries No. 3 and 4 for the original and finer mesh size are negligible and are shown in Figure. S1 and Figure S2, respectively. Similarly, since G_b-decoupled turbulence model predicts successful SST operation but not as the predictions are accurate predicted by the G_b-coupled turbulence model for geometries No. 10 and 11, two additional finer meshes (460,000 and 890,000 cells) are used for both geometries No. 10 and 11. Figure. S3 and Figure. S4 show that the difference among the three mesh sizes are negligible for geometries No. 10 and 11, respectively.

Additionally, the predictions of performance indicators, such as ESS, SBH and returned active sludge concentration (RAS) by the G_b-decoupled/coupled turbulence models among different mesh resolutions on geometries No. 3, 4, 10, and 11 are shown in Figure. S5 to Figure. S8, respectively. The results show that predictions by the G_b-decoupled and G_b-coupled turbulence models on the original mesh are similar to them on the finer mesh on each of these four SSTs.

2.3. *Model verification*

Since the measurements of the performance indicators (ESS and SBH) and velocity profiles for the Cases 2, 3a,b are available in Burt (2010), they are used to verify the model predictions.

2.3.1. *Performance indicators comparisons*

Fig. 2(a,b) shows the predictions of the ESS (Fig. 2a) and SBH (Fig. 2b) by the G_b-decoupled/coupled turbulence models for the Cases 2, 3a,b, respectively. It indicates that only the G_b-coupled turbulence model correctly predicts the performance indicators for the Case 2, while both the G_b-decoupled/coupled turbulence models correctly predict the performance indicators for the Case 3a and b. Therefore, the predictions of the velocity profiles by the G_b-decoupled turbulence model for the Case 3a and b are also added to compare the field measurements. The results are discussed in the next section.

2.3.2. Velocity profiles comparisons

Fig. 3 shows the comparisons between the prediction of the velocity profiles and the field measurements for Cases 2, 3a,b. Top, medium and bottom rows in the Fig. 2 represent the velocity profiles comparison for Cases 2, 3a,b, respectively. The predictions of the velocity profiles by the G_b-decoupled/coupled turbulence models are similar. Both the G_b-decoupled/coupled turbulence models reasonably predict the overall stream curvatures outside the stilling well.

Table 2 – Dimensions of circular SSTs.

Geometry	Values		
Geometry No.[a] Diameter of the clarifier	No. 1 35.0 m	No. 2 18.3 m	No. 3, 4 18.3 m
Surface area	962 m^2	263 m^2	263 m^2
Radius of the inlet pipe	0.5 m	0.4 m	0.4 m
Depth of side wall	4.1 m	1.8 m	1.8 m
Tank floor slope	10%	7.5%	7.5%
Hopper floor slope	/	60°	60°
Stilling/Center well diameter	6.0 m	5.49 m	1.65 m
Stilling/Center well depth	2.7 m	0.8 m	1.8 m
Stamford baffle depth	0.6 m	/	/
Stamford baffle length	1.7 m	/	/
Outboard launder	Peripheral launder	Peripheral launder	Peripheral launder

[a] Different SST geometries are numbered in Fig. 1.

Table 3 – Dimension of rectangular SSTs.

Geometry No.[a]	Tank length (m)	Tank depth (m)	Inlet height (m)	Outboard launder	Height of all the vertical baffles (m)	Length of all the horizontal baffles (m)	Horizontal distance of the vertical baffles (m)
No. 5					/	/	/
No. 6							/
No. 7							/
No. 8	60	4.5	0.5	Peripheral launder	2	3	/
No. 9							3
No. 10					/		
No. 11							

[a] Different SST geometries are numbered in Fig. 1.

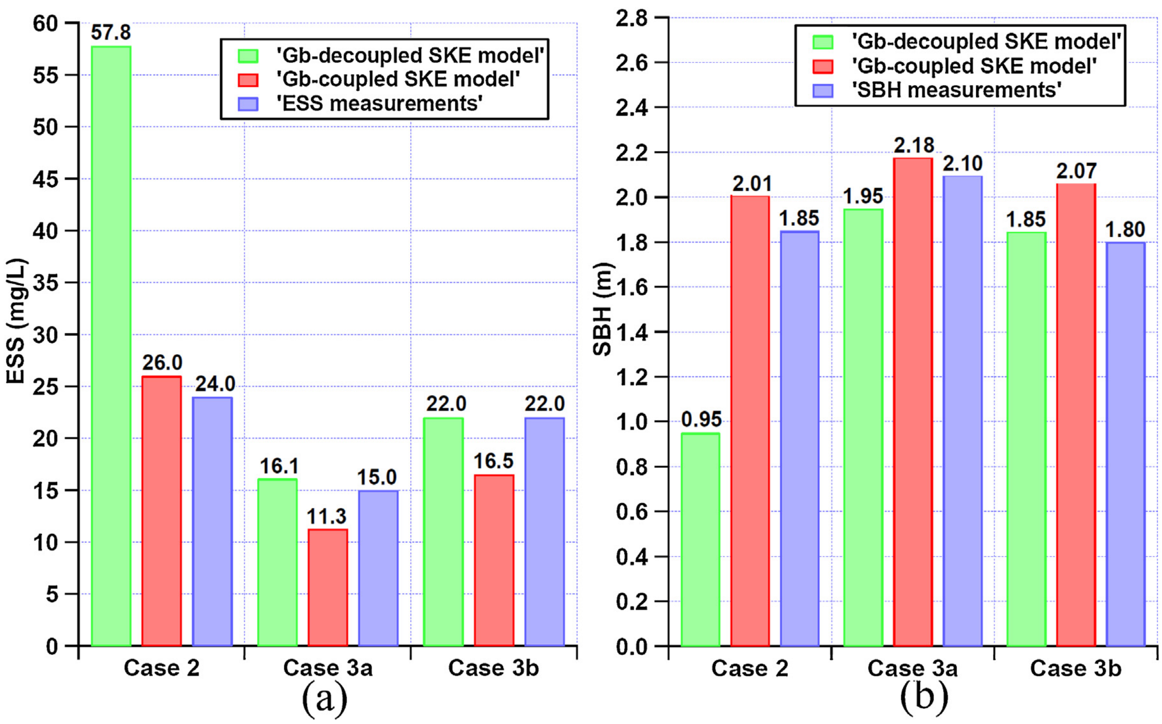

Fig. 2 – Comparisons of the performance indicators (a: ESS; b: SBH) between the model predictions and field observations for Cases 2, 3a,b, respectively.

3. Results and discussion

3.1. *Comparisons of predicted ESS by the G_b-decoupled/coupled turbulence models*

The predictions of the ESS by the G_b-decoupled/coupled turbulence models with these 13 cases are shown in Fig. 4. It shows that the change of the internal baffling structure, impacts the need for a coupled model, the results are divided into three different zones, based upon the dissipation in turbulence. Cases in Zone A the baffling produces only limited reductions in the effect of buoyancy on turbulence and simulations require a coupled model. In Zone C where there are larger reductions

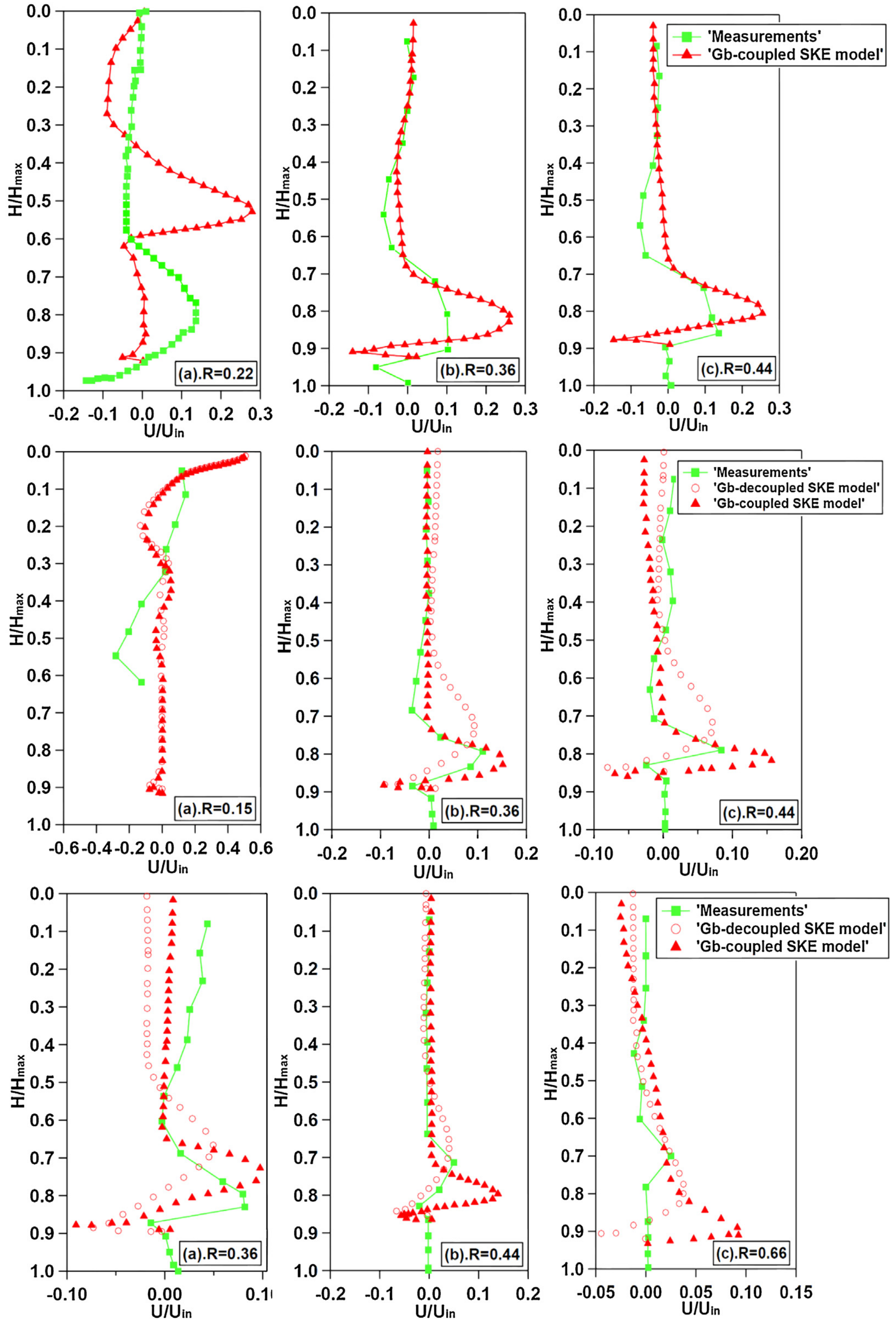

Fig. 3 – Comparisons of radial velocity profiles (m/s) between the model predictions and field measurements for Cases 2, 3a,b, respectively. R is the ratio between the radial distance of the vertical measurement location to the radius of tank. Case 2 (first row), Case 3a (second row), Case 3b (third row). The profiles of R = 0.22 for the Case 2 and R = 0.15 for the Case 3a are inside the stilling well. Other seven profiles are outside the stilling well. For Case 3a and b, the predictions of the buoyancy-decoupled turbulence model are also included.

in the effect of buoyancy on turbulence, either model can be used. Cases in Zone B may require a coupled model and the criteria are discussed later.

For the geometries No. 1, 2, 5–9, Cases 1, 2, 5–9, the predicted differences between the G_b-decoupled/coupled turbulence models are significant, and only the G_b-coupled turbulence model correctly predicts the ESS for these 7 cases. This implies that the effect of buoyancy on turbulence is strong in these geometries (Zone A).

For the geometries No. 10 and 11, Cases 10 and 11, the predictions of the ESS by both models are below the ESS limiting (30 mg/L), but the predictions differ by approximately 15 mg/L.

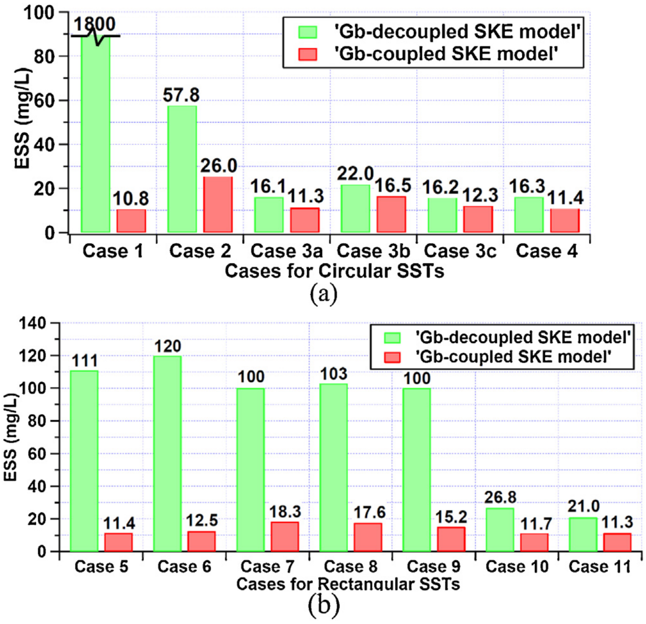

Fig. 4 – Predictions of the ESS by the G_b-decoupled/coupled turbulence models with these 13 cases (a: circular SSTs; b: rectangular SSTs).

The predictions of the ESS by the G_b-coupled turbulence model are approximately 12 mg/L while the predictions of the ESS by the G_b-decoupled turbulence model are close to the limiting ESS, 30 mg/L. This implies that the effect of buoyancy on turbulence is partially dissipated by the internal baffling (Zone B).

For the geometries No. 3, Case 3a,b,c and the geometries No. 4, Case 4, the predictions of the ESS by both models are similar, within 5 mg/L. This implies that the effect of buoyancy on turbulence is largely dissipated by the internal baffling (Zone C).

Additionally, the results of the geometries No. 1 and 2 are consistent with Gao and Stenstrom (2018b), where an inlet dissipating baffle alone cannot reduce the effect of buoyancy on turbulence under the normal loading conditions. Also, comparisons among the predicted ESS by the G_b-coupled turbulence model for the geometry No. 5 (the original rectangular geometry) and the geometries No. 6–9 (the first four modified rectangular geometries) show that a poor baffling structure can increase the ESS.

3.2. *Analyzing the effects of the internal baffling structures on turbulence*

In order to analyze the effects of the different baffling structures on turbulence, turbulent viscosity profiles are compared for these 13 different cases. Figs. 5 and 6 show the predictions of the turbulent viscosity by the G_b-decoupled turbulence model on the circular and rectangular SSTs, respectively. As shown in Fig. 5 for Case 3a–c and Case 4 in Zone C, the turbulence is reduced significantly by forcing the influent to flow through the baffling structure created by both the vertical and horizontal baffles. However, without the horizontal baffle (Cases 1 and 2), the turbulence is not dissipated and extends to the entire SST.

Also, in Fig. 6 for the Cases 10 and 11 in Zone B, the turbulence is reduced significantly by forcing the influent to flow through several vertical perforated walls on the depth of entire SST. However, without a baffling structure or with a poor baffling structure (Cases 5–9), the turbulence is prevailing in the SSTs and the strongest area is near the effluent weir.

The predictions of the turbulence viscosity profiles by the G_b-decoupled turbulence model directly show that the effects of the baffling structures on turbulence are varied. Good baffling structures can significantly dissipate the effect of buoyancy on turbulence, while the effect of buoyancy on turbulence is strong in the SSTs without a baffling structure or with poor baffling structures.

In order to quantitatively describe the influence of the baffling structure on the turbulence, the averaged turbulent kinetic energy (TKE) by the G_b-decoupled/coupled turbulence models for these 13 cases are calculated and the differences of the averaged TKE predicted by the G_b-decoupled/coupled

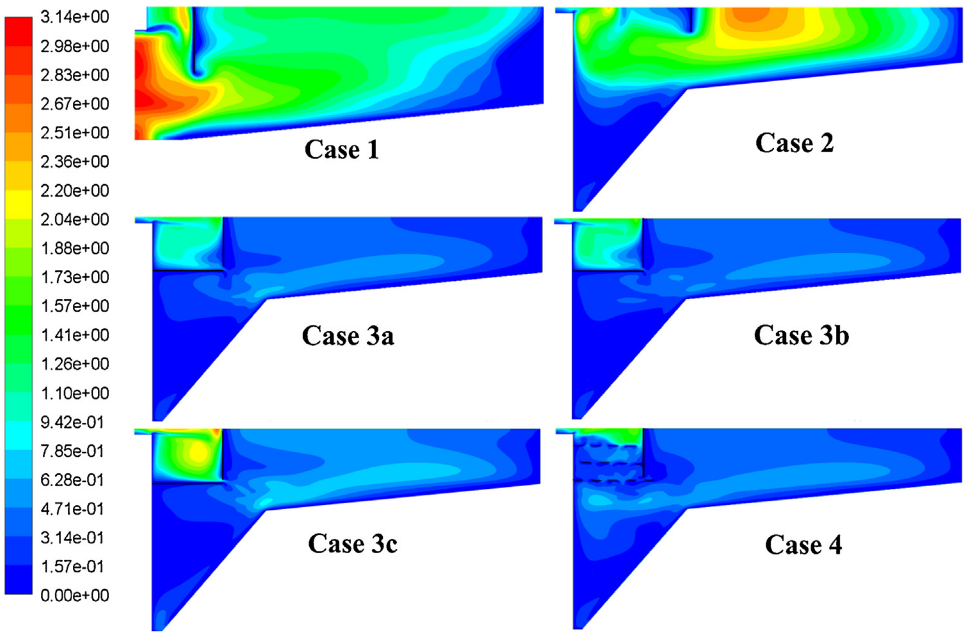

Fig. 5 – Predictions of the turbulent viscosity (kg/m-s) by the buoyancy-decoupled SKE models for the circular SSTs (Cases 1–4, respectively).

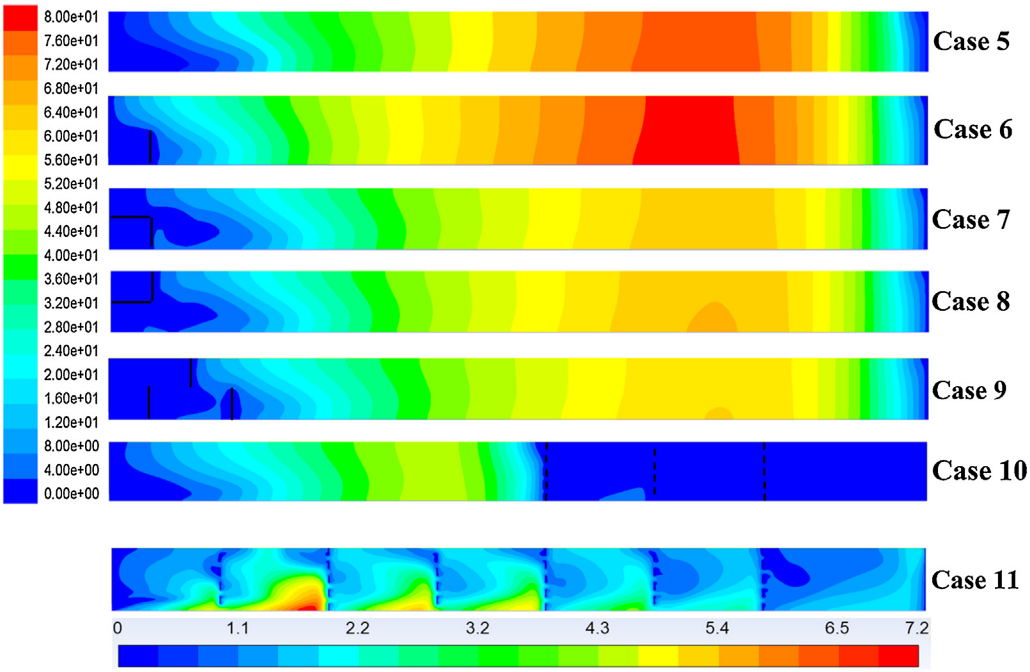

Fig. 6 – Predictions of the turbulent viscosity (kg/m-s) by the buoyancy-decoupled SKE models for the rectangular SSTs (Cases 5–11, respectively). The maximum turbulent viscosity in the Case 11 is less than 10% of it in the Cases 5–10. Therefore, in order to show the turbulence dissipation in the Case 11 clearly, a different colormap below the turbulent viscosity profile of the Case 11 is also applied in the Fig. 6.

Table 4 – Predictions of the averaged TKE (m^2/s^2) by the G_b-decoupled/coupled SKE models and calculations of their difference for each case. Three difference zones are classified based on the difference of the averaged TKE.

Cases No.	Geometry No. (Fig. 1)	Averaged TKE (m^2/s^2) $\times 1^{-4}$		Difference (%)	Different zones
Circular SSTs	Circular SSTs	G_b-decoupled	G_b-coupled		
1	1	3.39	2.10	38%	A
2	2	8.50	5.00	41%	A
3a	3	3.46	2.93	15%	C
3b	3	7.90	6.60	16%	C
3c	3	3.60	3.10	14%	C
4	4	3.65	3.00	18%	C
Rectangular SSTs	Rectangular SSTs				
5	5	6.33	0.37	94%	A
6	6	7.00	0.66	90%	A
7	7	6.20	1.10	82%	A
8	8	6.00	1.00	83%	A
9	9	5.70	0.60	89%	A
10	10	4.40	0.91	79%	B
11	11	1.10	0.27	75%	B

turbulence models are compared. The results are shown in Table 4 and indicate the differences of the averaged TKE by the G_b-decoupled/coupled SKE models. The differences between predicted TKE for both Cases 1 and 2 (Zone A) of the circular SSTs are 38–41%. For Case 3a–c and Case 4 (Zone C), the differences in TKE are less, 14–18%. The larger differences for Cases 1 and 2 indicate the need for a coupled model, but the smaller differences in Case 3a–c and Case 4 show that both models produce similar results.

For the rectangular SSTs, the differences of the averaged TKE by the G_b-decoupled/coupled SKE models for the Cases 5–9 are more than 90% (Zone A), and for the Cases 10 and 11 are approximately 80% (Zone B). These differences among the two sets of cases are much smaller than in the previous example.

The differences of the averaged TKE shown in Table 4 explain the prediction differences of the ESS by the G_b-decoupled/coupled SKE models for these 13 cases shown in Figs. 5 and 6. For the circular SSTs, since the averaged TKE is significantly dissipated for the cases in Zone C, the averaged TKE by the G_b-decoupled SKE model is similar to it predicted by the G_b-coupled SKE model. Therefore, both models predict similar ESS. For the rectangular SSTs, since the differences among the cases in Zones A and B are much smaller than the differences in the circular SSTs, the predictions of the ESS by the G_b-decoupled/coupled SKE models only show qualitatively agreement. For the cases in Zone A, which the difference of the averaged TKE by the G_b-decoupled/coupled SKE models is large, the ESS can only be correctly predicted by the G_b-coupled SKE model. Therefore, the difference of averaged TKE by the G_b-decoupled/coupled turbulence models can be used as the indicator to quantify the effects of the baffling structures and to show the G_b-decoupled turbulence model tends to work. Also, further study is needed to differentiate the performance of the G_b-decoupled/coupled SKE models for

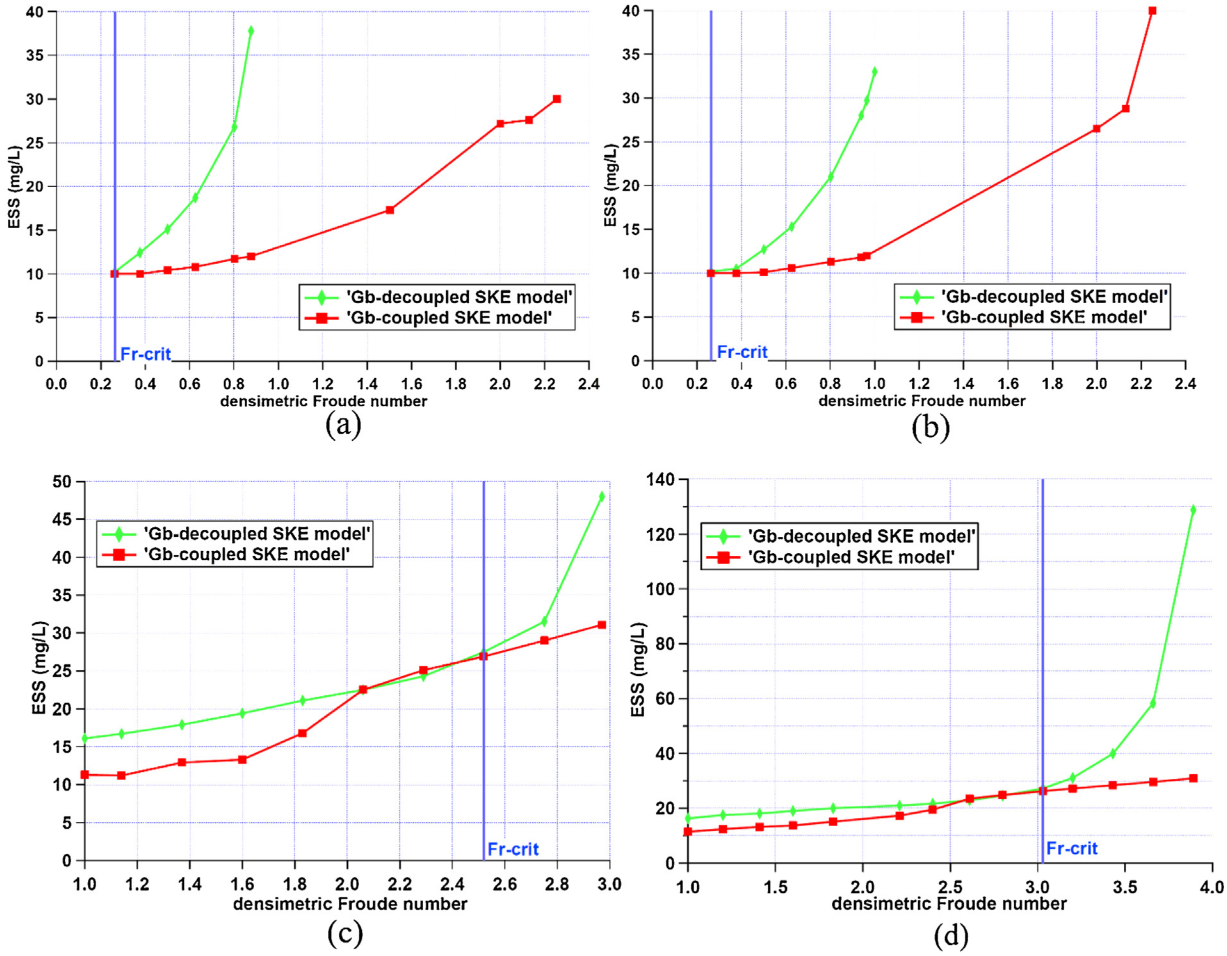

Fig. 7 – Predictions of the ESS as a function of inlet Fr in Zone B (geometries No. 10 (a) and 11 (b)) and in Zone C (geometries No. 3 (c) and 4 (d)).

the geometries in Zones B and C and is illustrated in the next section.

3.3. *CFD stress tests*

Since Fig. 4 shows that the G_b-decoupled turbulence model can also predict reasonable ESS for the SST geometries in Zones B and C, stress tests are simulated for these geometries by both models to compare the prediction of the SST capacities and to further distinguish the performance of the models. The stress tests are simulated by increasing the inlet densimetric Froude number (Fr).

Since the lowest surface overflow rate (SOR) applied for the cases in the Zones B and C is 0.332 m/h shown in Table 1, it is applied as the initial SOR for the CFD stress tests. Fr is then increased as the increase of the SOR and other conditions are kept constant.

Fig. 7(a)–(d) shows the predicted ESS as a function of inlet Fr for the geometries in Zones B and C. It shows that as the inlet Fr increases, there is a critical Fr (Fr-crit). Below Fr-crit, the predictions of the G_b-decoupled/coupled turbulence models are similar. As the inlet Fr exceeds the Fr-crit, the predicted ESS by these two models begins to diverge. Therefore, the inlet Fr can be used as the second indicator (indicator No. 2) to further differentiate the performance of these two models for the Zones B and C.

Fig. 7(a) and (b) shows that for geometries in Zone B, the values of the Fr-crit are both 0.263. The small value of Fr-crit indicates the predictions of the ESS by these two models are similar only when the Fr is very small and the predicted ESS diverges quickly with increasing Fr. When the G_b-decoupled turbulence model predicts the ESS over the limiting (30 mg/L) for the geometries in Zone B, the G_b-coupled turbulence model predicts approximately 12 mg/L ESS. For geometries in Zone C shown in Fig. 7(c) and (d), the values of the Fr-crit are 2.52 and 3.03. Fig. 7(c) and (d) shows that the predicted ESS by these two models respect to the Fr-crit are close to the ESS limiting (30 mg/L), which indicates that both models can correctly predict the ESS before it reaches the limiting value.

The CFD stress tests show that both models work in Zone C from the low flow conditions to the limiting flow conditions, whereas the G_b-decoupled turbulence model works well when the buoyancy-coupled turbulence model for low flow conditions in Zone B. The results are consistent with the reduction of the difference of the averaged TKE (indicator No. 1) showing in Table 4, which the geometries in Zone C fully dissipate the effect of buoyancy on turbulence, while the geometries in Zone B partially dissipate the effect of buoyancy on turbulence.

4. Conclusions

In this paper, a Fluent-based 2D SST model is used to generalize the effects of internal baffling structures on the buoyancy-induced turbulence. Eleven SST geometries, including four circular SST geometries and seven rectangular SST geometries, are evaluated. Predictions of the ESS by the buoyancy-decoupled and buoyancy-coupled SKE models on these eleven SST geometries are compared, and the effects of

Table 5 – Summary of all the cases and relevant geometries which can be correctly predicted by the G_b-decoupled or G_b-coupled turbulence models.

Correct predictions by G_b-decoupled or -coupled models	Zones	Cases No.	Geometries No.
G_b-coupled turbulence model only	A	1, 2, 5–9	1, 2, 5–9
G_b-decoupled turbulence model (partially[a]) & G_b-coupled turbulence model	B	10, 11	10, 11
G_b-decoupled turbulence model (fully[a]) & G_b-coupled turbulence model	C	3a–c, 4	3, 4

[a] Partial means the prediction of the G_b-decoupled turbulence model is similar to the prediction of the G_b-decoupled turbulence model only if the inlet Fr is small. Fully means the prediction of the G_b-decoupled turbulence model is similar to the prediction of the G_b-decoupled turbulence model from the low inlet Fr to the limiting Fr (ESS ≥ 30 mg/L).

the internal baffling structures on the turbulence properties, such as turbulent viscosity and averaged TKE, are analyzed and quantified. The results show that the effects of the baffling structures can be divided into three different zones, which negligibly (Zone A), partially (Zone B), and fully (Zone C) dissipate the turbulence. Furthermore, CFD stress tests are simulated on the geometries in the Zones B and C by both buoyancy-decoupled and buoyancy-coupled turbulence models and the inlet densimetric Froude number is applied to further differentiate the performance of these two models in Zones B and C.

Based on the simulation results on these different SST geometries, the following conclusions are made:

- The effects of the SST baffling structures on the buoyancy-induced turbulence are varied on both circular and rectangular SSTs. Good baffling structures can significantly dissipate the effect of buoyancy on turbulence, while the effect of buoyancy on turbulence is strong in the SST without a baffling structure or with poor baffling structures.
- The difference of the averaged TKE by the buoyancy-decoupled/coupled SKE models can be used as the first indicator (indicator No. 1) to quantify the influence of the baffling structure on the effect of buoyancy on turbulence and to differentiate the performance of these two turbulence models.
- The inlet densimetric Froude number can be used as the second indicator (indicator No. 2) to further distinguish the performance of the buoyancy-decoupled/coupled SKE models for the SST geometries in Zones B and C. Below the critical inlet Fr (Fr-crit), both models predict similar results. As soon as the inlet Fr exceeds Fr-crit, the predictions of the models gradually diverge.
- Only the buoyancy-coupled turbulence model can correctly predict the performance of the SST geometries in Zone A, while the buoyancy-decoupled turbulence model works as well as the buoyancy-coupled turbulence model under the low flow conditions in Zone B, and both models work from the low flow conditions to the limiting flow conditions in Zone C. This point is also summarized in Table 5.

5. Future research

The applicability of some more advanced turbulence models, such as Reynold stress and LES models, have not yet been validated for SSTs partially due to the development of their damping term on the effect of buoyancy on turbulence. However, for the geometries which can also be correctly predicted without implementation the G_b in the turbulence model, the performance of these more advanced turbulence models can be compared with the turbulence models in the k-epsilon family in the future research.

Appendix A. Supplementary data

Supplementary material related to this article can be found, in the online version, at doi:https://doi.org/10.1016/j.cherd.2019.01.015.

References

Burt, D.J., 2010. Improved Design of Settling Tanks Using an Extended Drift Flux Model. (Ph.D. thesis). University of Bristol, UK.

Dahl, C., 1993. Numerical Modelling of Flow and Settling in Secondary Settling Tanks. Aalborg University, Department of Civil Engineering.

Das, S., Bai, H., Wu, C., Kao, J.-H., Barney, B., Kidd, M., Kuettel, M., 2016. Improving the performance of industrial clarifiers using three-dimensional computational fluid dynamics. Eng. Appl. Comput. Fluid Mech. 10 (1), 130–144.

Devantier, B.A., Larock, B.E., 1986. Modelling a recirculating density driven turbulent flow. Int. J. Numer. Methods Fluids 6 (4), 241–253.

Gao, H., Stenstrom, M.K., 2017. Computational Fluid Dynamics Applied to Secondary Clarifier Analysis., pp. 301–315.

Gao, H., Stenstrom, M.K., 2018a. Evaluation of three turbulence models in predicting of the hydrodynamics of a secondary sedimentation tank. Water Res. 143 (June), 445–456.

Gao, H., Stenstrom, M.K., 2018b. Turbulence and inter-phase mass diffusion assumptions on performance of secondary settling tanks. Water Environ. Res. 91 (October), 1–10.

Gong, M., Xanthos, S., Ramalingam, K., Fillos, J., Beckmann, K., Deur, A., McCorquodale, J.A., 2011. Development of a flocculation sub-model for a 3-D CFD model based on rectangular settling tanks. Water Sci. Technol. 63 (2), 213–219.

Imam, E., McCorquodale, J.A., Bewtra, J.K., 1983. Numerical modeling of sedimentation tanks. J. Hydraul. Eng. 109 (12), 1740–1754.

Krebs, P., 1991. The hydraulics of final settling tanks. Water Sci. Technol. 23 (4–6), 1037–1046.

Krebs, P., Vischer, D., Gujer, W., 1992. Improvement of secondary clarifiers efficiency by porous walls. Water Sci. Technol. 26 (5–6), 1147–1156.

Krebs, P., Vischer, D., Gujer, W., 1995. Inlet-structure design for final clarifiers. J. Environ. Eng. 121 (8), 558–564.

Krebs, P., Stamou, A., Garcia-Heras, J.L., Rodi, W., 1996. Influence of inlet and outlet configuration on the flow in secondary clarifiers. Water Sci. Technol. 34 (5–6), 1–9.

Lakehal, D., Krebs, P., Krijgsman, J., Rodi, W., 1999. Computing shear flow and sludge blanket in secondary clarifiers. J. Hydraul. Eng. 125 (3), 253–262.

Larsen, P., 1977. On the Hydraulics of Rectangular Settling Basins: Experimental and Theoretical Studies. Department of Water Resources Engineering, Lund Institute of Technology.

Li, B., Stenstrom, M.K., 2014. Research advances and challenges in one-dimensional modeling of secondary settling tanks—a critical review. Water Res. 65, 40–63.

Lyn, D., Stamou, A., Rodi, W., 1992. Density currents and shear-induced flocculation in sedimentation tanks. J. Hydraul. Eng. 118 (6), 849–867.

McCorquodale, J.A., La Motta, E., Griborio, A., Georgiou, I., Homes, J., 2004. Development of Software for Modeling Activated Sludge Clarifier System. Technology Transfer Report Submitted to US EPA, Schielder Urban Environmental System Center. University of New Orleans, New Orleans, LA, USA.
Parker, D.S., Merlo, R.P., Jimenez, J.A., Wahlberg, E.J., 2008. Analyzing wet weather flow management using state of the art tools. Water Sci. Technol. 57 (8), 1247–1251.
Patziger, M., 2016. Computational fluid dynamics investigation of shallow circular secondary settling tanks: inlet geometry and performance indicators. Chem. Eng. Res. Des. 112, 122–131.
Patziger, M., Kiss, K., 2015. Analysis of suspended solids transport processes in primary settling tanks. Water Sci. Technol. 72 (1), 1–9.
Patziger, M., Kainz, H., Hunze, M., Jozsa, J., 2008. Analysing sludge balance in activated sludge systems with a novel mass transport model. Water Sci. Technol. 57 (9), 1413–1419.
Patziger, M., Kainz, H., Hunze, M., Jozsa, J., 2012. Influence of secondary settling tank performance on suspended solids mass balance in activated sludge systems. Water Res. 46 (7), 2415–2424.
Ramalingam, K., Xanthos, S., Gong, M., Fillos, J., Beckmann, K., Deur, A., McCorquodale, J.A., 2012. Critical modeling parameters identified for 3D CFD modeling of rectangular final settling tanks for New York City wastewater treatment plants. Water Sci. Technol. 65 (6), 1087–1094.
Ramin, E., Wagner, D.S., Yde, L., Binning, P.J., Rasmussen, M.R., Mikkelsen, P.S., Plosz, B.G., 2014. A new settling velocity model to describe secondary sedimentation. Water Res. 66, 447–458.
Rodi, W., 1993. Turbulence Models and Their Application in Hydraulics. CRC Press.
Shahrokhi, M., Rostami, F., Md Said, M.A., Syafalni, 2013. Numerical modeling of baffle location effects on the flow pattern of primary sedimentation tanks. Appl. Math. Model. 37 (6), 4486–4496.
Tamayol, A., Firoozabadi, B., Ashjari, M., 2009. Hydrodynamics of secondary settling tanks and increasing their performance using baffles. J. Environ. Eng. 136 (1), 32–39.
Vitasovic, Z.C., Zhou, S., McCorquodale, J.A., Lingren, K., 1997. Secondary clarifier analysis using data from the Clarifier Research Technical Committee protocol. Water Environ. Res. 69 (5), 999–1007.
Weiss, M., Plósz, B.G., Essemiani, K., Meinhold, J., 2007. Suction-lift sludge removal and non-Newtonian flow behaviour in circular secondary clarifiers: numerical modelling and measurements. J. Chem. Eng. 132 (1–3), 241–255.
Xanthos, S., Gong, M., Ramalingam, K., Fillos, J., Deur, A., Beckmann, K., McCorquodale, J.A., 2010. Performance assessment of secondary settling tanks using CFD modeling. Water Resour. Manag. 25 (4), 1169–1182.
Xanthos, S., Ramalingam, K., Lipke, S., McKenna, B., Fillos, J., 2013. Implementation of CFD modeling in the performance assessment and optimization of secondary clarifiers: the PVSC case study. Water Sci. Technol. 68 (9), 1901–1913.
Zhou, S., McCorquodale, J.A., 1992a. Influence of skirt radius on performance of circular clarifier with density stratification. Int. J. Numer. Meth. Fluid. 14 (8), 919–934.
Zhou, S., McCorquodale, J.A., 1992b. Mathematical modelling of a circular clarifier. Can. J. Civ. Eng. 19 (3), 365–374.
Zhou, S., McCorquodale, J.A., 1992c. Modeling of rectangular settling tanks. J. Hydraul. Eng. 118 (10), 1391–1405.
Zhou, S., McCorquodale, J.A., Vitasovic, Z., 1992. Influences of density on circular clarifiers with baffles. J. Environ. Eng. 118 (6), 829–847.